42.1: A Class of Micromachined Gyroscopes with Increased Parametric Space

Cenk Acar
Microsystems Laboratory
Mechanical and Aerospace Engineering Dept.
University of California at Irvine
Irvine, CA, USA
cacar@uci.edu

Andrei M. Shkel
Microsystems Laboratory
Mechanical and Aerospace Engineering Dept.
University of California at Irvine
Irvine, CA, USA
ashkel@uci.edu

Abstract
This paper reports a design concept for MEMS gyroscopes based on increasing the degrees-of-freedom of the oscillatory system by the use of two independently oscillating interconnected proof masses. The 4-DOF dynamical system eliminates the necessity for mode-matching due to its wide operation frequency range, and reduces the damping sensitivity problem by operating away from resonance.Thus, inherent disturbance rejection is achieved, providing reduced sensitivity to structural and thermal parameter fluctuations. The basic operational principles of the design concept were experimentally demonstrated, including the wide operation frequency band, and dynamic amplification providing high oscillation amplitudes without resonance.

Keywords
MEMS, inertial sensors, micromachined gyroscopes.

INTRODUCTION
Even though there is an extensive variety of micromachined gyroscope designs and operation principles, almost all of the reported micromachined gyroscopes use vibrating mechanical elements to sense rotation [1]. Vibratory gyroscopes are based on the transfer of energy between two vibration modes of a structure caused by Coriolis acceleration, which is induced in the presence of an input rotation rate.

The conventional micromachined rate gyroscopes operate on the vibratory principle of a 2-DOF system with a single proof mass, which is sustained in resonance in drive direction, and excited by the rotation-induced Coriolis force in the sense direction (Fig. 2a). When the mass is driven along x-axis at the drive frequency ω_d with a constant amplitude sinusoidal drive force $F_d = F_o sin\omega_d t$, the equations of motion are:

$$\begin{aligned} m\ddot{x} + c_x\dot{x} + k_x x &= F_o sin\omega_d t + 2m\Omega_z\dot{y} \\ m\ddot{y} + c_y\dot{y} + k_y y &= -2m\Omega_z\dot{x} \end{aligned} \quad (1)$$

assuming the angular rate input Ω_z is constant, and Ω_z^2 is negligibly small. The 2-DOF dynamical system will have two distinct resonant frequencies: $\omega_x = \sqrt{k_x/m}$ in the drive direction, and $\omega_y = \sqrt{k_y/m}$ in the sense direction.

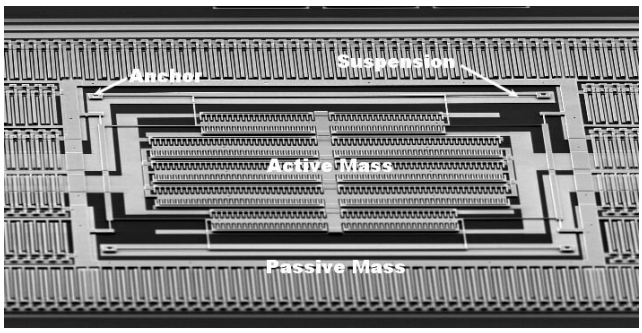

Figure 1. Scanning Electron Microscope photograph of a prototype 4-DOF gyroscope.

In an ideal gyroscope, the rotation-induced Coriolis force $F_c = 2m\Omega_z\dot{x}$, which is proportional to the drive direction oscillation amplitude, is the only driving force in the sense direction. If $\omega_d = \omega_x$, then system is in resonance in the drive direction, and a high sense direction amplitude is achieved due to the increased Coriolis force F_c. If $\omega_d = \omega_y$, then system is in resonance in the sense direction, providing high sense direction amplitudes. Thus, when $\omega_x \neq \omega_y$, the frequency response of the 2-DOF system has two resonant peaks, one at ω_x, and another at ω_y. When the drive and sense resonant frequencies are matched, i.e., $\omega_x = \omega_y$, the frequency response of the 2-DOF system has one combined resonant peak, which will provide a much larger response amplitude due to coinciding drive and sense resonance peaks (Fig. 2b). Thus, drive and sense resonant frequencies are typically designed and electronically tuned to match, and the device is controlled to operate at or near the peak of the resonance curve.

However, this resonance dependent approach results in a response with narrow bandwidth, and consequently, high sensitivity to variations in system parameters. The requirement to keep the drive and sense resonance frequencies matched in a very narrow frequency band in the presence of perturbations is the major factor limiting the robustness of the conventional gyroscopes. Under high quality factor conditions the gain is high, however, the bandwidth is extremely narrow. In addition, the gain is affected significantly by fluctuations in damping conditions.

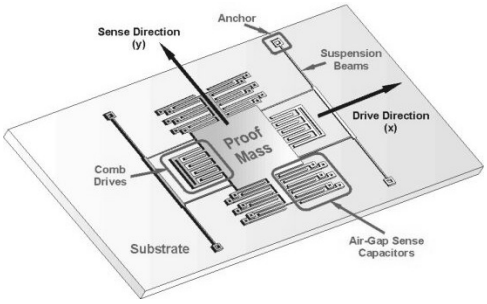

(a)

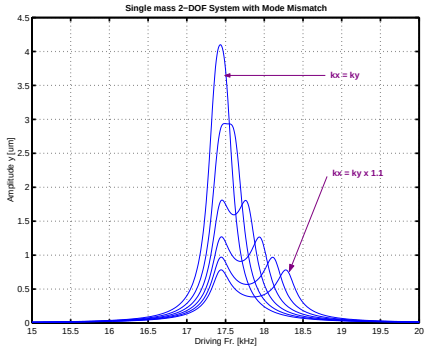

(b)

Figure 2. (a) A conceptual MEMS implementation of a conventional single-mass rate gyroscope. (b) The response of the overall 2-DOF system with varying drive and sense stiffness mismatch. The highest response corresponds to the case where the drive and sense modes are matched, and the response amplitude diminishes as the mismatch increases.

Fabrication imperfections are also inevitable, and both the geometry and the material properties of MEMS devices are affected by etching processes, deposition conditions, and residual stresses. Our experimental results demonstrated possible deviations of over 20% from the designed system parameters due to these effects. Compensation for the disturbances as a result of fabrication imperfections and temperature variations require sophisticated control architectures.

Micromachined gyroscopes could potentially provide accurate rotation measurements leading to a wide range of applications including navigation and guidance systems, automotive safety systems, and consumer electronics. However, truly low-cost and high-performance devices are not on the market yet, and the current state of the art micromachined gyroscopes require orders of magnitude improvement in performance, stability, and robustness due to the discussed limitations. In this paper, a design concept that provides increased robustness and stability is presented, and system dynamics and control issues are discussed. Details on the fabricated prototypes are followed by the preliminary experimental results verifying the feasibility of implementation of the design concept.

THE 4-DOF SYSTEM APPROACH

To eliminate the limitations of the conventional micromachined gyroscopes, we propose a design concept that suggests the use of an oscillatory system with increased parametric space, providing a more favorable frequency response. The proposed design concept is based on increasing the degrees-of-freedom of the oscillatory system by the use of two independently oscillating interconnected proof masses (Fig. 1 and Fig. 3a). With the 4-DOF system, inherent disturbance rejection is achieved due to the wide operation frequency range of the dynamic system, providing reduced sensitivity to structural and thermal parameter fluctuations. By requiring less demanding active control strategies for operation under presence of perturbations, complexity of the control electronics can be shifted to dynamical system complexity. Thus, the approach is expected to provide low-cost solutions to applications with large fluctuations in operation conditions.

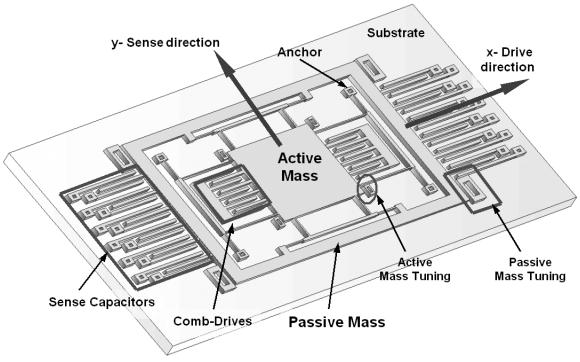

(a)

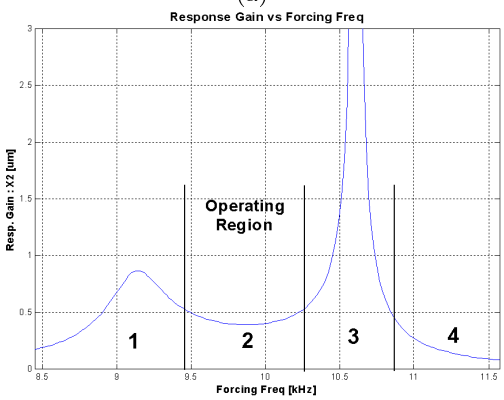

(b)

Figure 3. (a) A MEMS implementation of the 4-DOF design concept. The active mass is electrostatically driven to achieve mechanical amplification by the passive mass, and the Coriolis response of the passive mass in the sense direction is detected. (b) Response of the dual-mass system has the flat operating region between the two resonance peaks.

In contrast to the conventional micromachined gyroscopes, the proposed design approach utilizes two vibrating proof masses suspended above the substrate, which form a 4 degrees-of-freedom (DOF) dynamic system. The suspension system renders both of the proof masses free to oscillate in the drive and sense directions. The first mass is forced to oscillate in the drive direction, and this forced oscillation is amplified by the second mass. The response of the second mass to the Coriolis force in the orthogonal direction is sensed. With appropriate selection of dynamical system parameters, a Coriolis response with two resonant peaks, and a flat region between peaks can be obtained. Nominal operation of the device is in the flat region of the response, where the gain is relatively insensitive to parameter fluctuations (Fig. 3b). In this flat region, a 1% variation in natural frequencies of the system results in only 0.8% error in the output signal, which is less than 4% of the error experienced with a conventional design under similar operating conditions [9]. Thus, the device can be operated in a much wider frequency band with insignificant change in the gain, in the presence of perturbations. Moreover, since the proposed device utilizes dynamic amplification of mechanical motion instead of in-resonance operation, the response is insensitive to damping changes in the operation region [12].

Since the approach overcomes the mode-matching and damping sensitivity problems of the resonance-dependent gyroscopes by operating in the flat region, over 50% of the gain is sacrificed for robustness. However, by utilizing dynamic amplification to achieve high oscillation amplitudes without resonance, gains within measurable limits are obtained. For example, over $0.1\mu m$ oscillation amplitudes in the sense mode are possible for a 1deg/sec rotation input, depending on design and fabrication parameters, and operation conditions.

4-DOF SYSTEM DYNAMICS, AND CONTROL CHALLENGES

When the active and passive masses (Fig. 3a), which are subject to an angular rate of Ω_z about the axis normal to the plane of operation (z-axis), are observed in the non-inertial rotating gyroscope frame, the equations of motion for the two-mass system along the x-axis and y-axis become [12]:

$$\begin{aligned} m_1\ddot{x_1} + c_{1x}\dot{x_1} + k_{1x}x_1 = k_{2x}(x_2 - x_1) + m_1\Omega_z^2 x_1 + \\ c_{2x}(\dot{x_2} - \dot{x_1}) - 2m_1\Omega_z\dot{y_1} - m_1\dot{\Omega_z}y_1 + F_d(t) \\ m_2\ddot{x_2} + c_{2x}(\dot{x_2} - \dot{x_1}) + k_{2x}(x_2 - x_1) = \\ m_2\Omega_z^2 x_2 - 2m_2\Omega_z\dot{y_2} - m_2\dot{\Omega_z}y_2 \\ m_1\ddot{y_1} + c_{1y}\dot{y_1} + k_{1y}y_1 = k_{2y}(y_2 - y_1) + \\ c_{2y}(\dot{y_2} - \dot{y_1}) + m_1\Omega_z^2 y_1 + 2m_1\Omega_z\dot{x_1} + m_1\dot{\Omega_z}x_1 \\ m_2\ddot{y_2} + c_{2y}(\dot{y_2} - \dot{y_1}) + k_{2y}(y_2 - y_1) = \\ m_2\Omega_z^2 y_2 + 2m_2\Omega_z\dot{x_2} + m_2\dot{\Omega_z}x_2. \quad (2) \end{aligned}$$

where $F_d(t)$ is the driving electrostatic force applied to the active mass at the driving frequency ω_d, and Ω_z is the angular velocity applied to the gyroscope about the z-axis.

Since the Coriolis response of the second mass in the sense direction is directly correlated with the drive oscillation amplitude, it is crucial that the second mass is driven into forced oscillation in drive direction with a known constant amplitude. Thus, the primary task of the control electronics is to assure constant amplitude oscillation for the second mass with the required driving frequency.

Moreover, micromachined gyroscopes are sensitive not only to the measured angular rate, but also to fabrication imperfections and undesirable excitations. Fabrication imperfections introduce perturbations and anisoelasticities to the dynamical system, limiting the sensor performance. Thus, the other major task of the control system is to compensate for these imperfections.

Control of Oscillations in Drive Mode

The Coriolis force which excites the second mass in the sense direction is described by $F_{Coriolis} = 2m_2\Omega\dot{x_2}$. Since the Coriolis force is proportional to the linear velocity of the second mass, it is also proportional to the oscillation amplitude. Thus, it is vital for the drive control electronics to keep a constant known drive-direction oscillation amplitude of the second mass for accurate angular rate measurement.

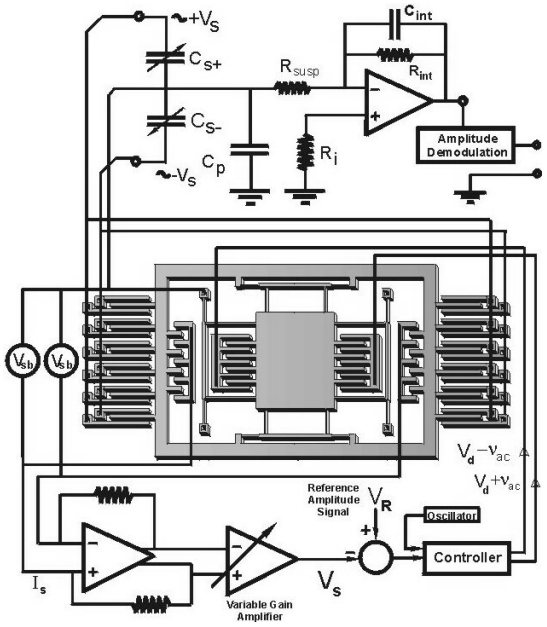

Figure 4. Closed-loop driving scheme of dual-mass gyroscope.

To provide the feedback signal for achieving the desired oscillation amplitude, comb structures have to be built on the second mass (Figure 4). By incorporating a

trans-resistance amplifier into the control loop, the displacement current generated by the oscillating second mass is converted to an output voltage. This output voltage V_s is then compared to a reference voltage V_R, which determines the desired oscillation amplitude.
The current due to capacitance change in the comb drives with the motion of the second mass can be expressed in terms of linear velocity of the second mass ν_2, capacitance change due to deflection $\frac{\partial C}{\partial x}$, deflection sensing bias voltage V_{sb}, and the amplitude of oscillation X_2 as:

$$I_s = V_{sb}\frac{\partial C}{\partial x}\nu_2(t) = V_{sb}\frac{\partial C}{\partial x}X_2\omega_{drive}\sin(\omega_{drive}t) \quad (3)$$

With this current input, the output voltage from the trans-resistance amplifier, which will be compared to the reference input to get the error signal, is:

$$V_S = V_{sb} + RV_{sb}\frac{\partial C}{\partial x}X_2\omega_{drive}\sin(\omega_{drive}t) \quad (4)$$

where R is the trans-resistance amplifier gain. The gain R is adjusted in conjunction with the reference voltage V_R. The obtained error signal $e = V_R - V_s$ is then fed into the controller. By summing the output voltage of the controller V_{cont} and the nominal drive voltage V_{nom}, the controlled total drive voltage is obtained to be fed to the comb-drives. A proportional-integral controller with frequency modulator drives the first mass with the required voltage amplitude and frequency to converge the error signal amplitude to zero. The controller receives the clock signal from an oscillator which will set the driving frequency ω_{drive} to the operational frequency.

Compensation of Fabrication Imperfections

Because of slight asymmetries in gyroscope structure due to random scatter of fabrication imperfections and residual stresses, the drive and sense axes in the gyroscope will not perfectly coincide with the principle axes of elasticity. Due to lack of perfect alignment of the intended and the actual principle axes of oscillation, anisoelasticity in the gyroscope structure occurs, causing dynamic cross-coupling between the drive and sense directions. The resulting dynamic cross-coupling stiffness and damping terms are the major factors that limit the performance of the gyroscope [14].
For the 4-DOF system, the suspension system consists of two separate parts, which are the flexures between the active mass and the substrate, and flexures between the passive and active masses. The asymmetric imperfections can be modeled as an angle of elasticity ε_1 for substrate-active mass suspension, and ε_2 for the suspension between the active mass and the passive mass (Fig. 5). These angles will result in cross-coupling stiffness terms k_{1xy} and k_{2xy}, and the stiffness terms $k_{1xx}, k_{2xx}, k_{1yy}$, and k_{2yy} deviated from the intended values.

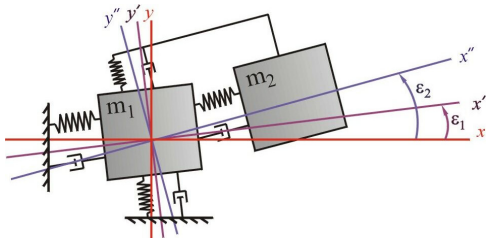

Figure 5. Modeling of asymmetric imperfections in the 4-DOF gyroscope. The asymmetric imperfections can be modeled as an angle of elasticity ε_1 for substrate-active mass suspension, and ε_2 for the suspension between the active mass and the passive mass .

$$k_{ixx} = \frac{k_{ix}+k_{iy}}{2} + \frac{k_{ix}-k_{iy}}{2}cos(2\varepsilon_i)$$
$$k_{iyy} = \frac{k_{ix}+k_{iy}}{2} - \frac{k_{ix}-k_{iy}}{2}cos(2\varepsilon_i)$$
$$k_{ixy} = \frac{k_{ix}-k_{iy}}{2}sin(2\varepsilon_i) \quad (5)$$

for i=1 and 2. When the anisoelasticity angles ε_1 and ε_2 are introduced to the system, phase changes are observed most significantly on x_1. Thus, anisoelasticity has the most effect on the trajectory of active mass, which is not the sensing element of the gyroscope. However, when critical values of the anisoelasticity angles ε_1 and ε_2 are exceeded, the passive mass sense amplitude increases, burying the contained Coriolis signal. It is also observed that the system is relatively immune to anisoelasticity in the active mass suspension, while the mass trajectories and gyroscope response is affected dramatically with anisoelasticity in the passive mass suspension (Fig. 6).

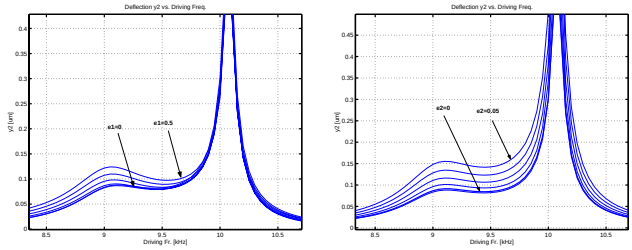

(a) (b)

Figure 6. Effect of (a) ε_1 variation, and (b) ε_2 variation on 4-DOF system response.

FABRICATION OF A PROTOTYPE

The design concept of a wide-bandwidth micromachined z-axis gyroscope can be implemented in any standard surface or bulk micromachining process, with at least one free-standing structural layer, one sacrificial layer, and one structural layer for electrical interconnects. The

initial prototype 4-DOF gyroscopes were fabricated in a two-layer 2 μm surface micromachining process, where polysilicon is used as the structural material, LPCVD deposited oxide (PSG) as the sacrificial layer, and silicon nitride as electrical isolation between the polysilicon and the substrate. The proof masses, and the suspension system are formed in the second structural polysilicon layer (Poly1), together with the interdigitated comb-drives structures which are used to drive the first mass into oscillations in the drive direction, and the air-gap capacitors which are used to sense the response of the second mass in the sense direction. The electrical connections are formed using the first structural polysilicon layer (Poly0) deposited on the nitride coating layer [13]. The masses are suspended over the substrate with a $2\mu m$ clearance, which is the thickness of the first sacrificial layer, Oxide1.

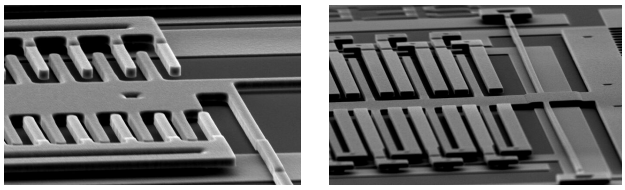

(a) (b)

Figure 7. Scanning Electron Microscope (SEM) photograph of (a) the comb-drives, and (b) the air-gap sense capacitors.

The first step of the fabrication process is deposition of a silicon nitride layer on the silicon substrate as an electrical isolation layer. This is followed directly by the deposition of Poly0, the first 500 nm thick structural polysilicon film. Poly0 is then photolithographycally patterned by photoresist coating, exposing, developing and reactive ion etching. A 2.0 μm phosphosilicate glass (PSG) sacrificial layer, Oxide1, is then deposited by LPCVD. This PSG sacrificial layer is removed at the end of the process to free the first mechanical layer of polysilicon. The sacrificial layer is lithographically patterned with the dimples mask and the dimples are transferred into the sacrificial PSG layer by RIE. The wafers are then patterned with the third mask layer, the anchor mask, and reactive ion etched, providing anchor holes that are filled by the second polysilicon layer (Poly1). After etching anchors, the second structural layer of polysilicon is deposited. This structural layer has a thickness of 2.0 μm, and the moving structures including the proof mass, suspension system and the capacitors are lithographically formed in this layer. Finally, the wafer is diced, and the structures are released in HF solution [13].

PRELIMINARY EXPERIMENTAL VERIFICATION OF THE DESIGN CONCEPT

The dominant Coriolis force exciting the system in the sense direction,

$$F_{Coriolis} = 2m_2\Omega\dot{x}_2 = 2m_2\Omega\omega_d x_{2o}, \qquad (6)$$

is proportional to the oscillation amplitude of the passive mass in the drive direction, x_{2o}. Thus, to assure an accurate angular rate measurement, it is crucial that the sensing element of the gyroscope is sustained in a constant amplitude oscillation in the drive direction. Preliminary experiments conducted on prototype dual-mass gyroscopes indicated a driving frequency range of over 2 kHz within where the drive direction oscillation amplitude varies by 10% (Fig. 8). A conventional gyroscope design with similar geometry exhibited less than 200 Hz driving frequency range for 10% gain variation under same operating conditions, which is over 1.8 kHz less than dual-mass design operation range, verifying the drastically improved robustness of the dual-mass design.

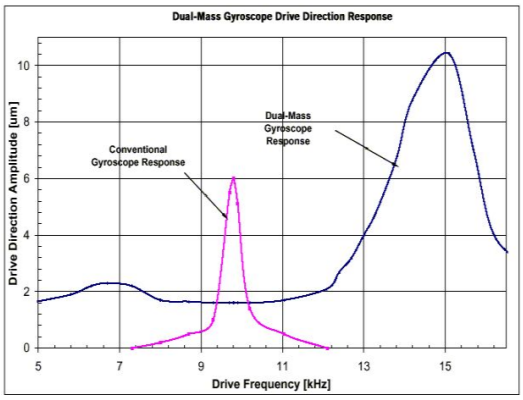

Figure 8. Experimental verification of the wide constant-amplitude operation frequency band. 4-DOF system provides a constant-amplitude oscillation frequency band over 10 times larger than conventional gyroscopes under same operation conditions.

The prototype gyroscopes also successfully demonstrated the mechanical amplification of the active mass oscillation by the passive mass, which is the sensing element of the gyroscope. The drive direction oscillation amplitude of the passive mass, which is one of the major parameters determining gyroscope performance, was demonstrated to be over 15 times larger than the active mass under atmospheric pressure (Fig. 9). At the antiresonance frequency, the active mass drive amplitude (A_1 in Fig. 9) was observed to be less than $0.1\mu m$, while the passive mass amplitude (A_2 in Fig. 9) reached $1.4\mu m$. This provides large drive-direction oscillation amplitudes of the sensing element, and thus, high Coriolis forces without the necessity of drive-direction resonance.

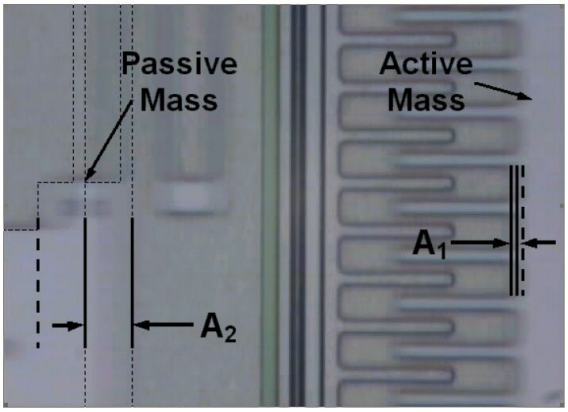

Figure 9. Demonstration of mechanical amplification in drive direction. The oscillation blur of the passive mass is highlighted on the left. At the antiresonance frequency, the passive mass amplitude is over an order of magnitude larger than the active mass amplitude.

CONCLUSION

In this paper, a 4-DOF micromachined vibratory rate gyroscope design concept was presented, which addresses the limitations of the conventional micromachined gyroscope due to in-resonance operation. The proposed design concept suggests the use of two coupled independently vibrating proof masses to form a 4-DOF dynamical system, which has a Coriolis response with two resonance peaks, and a flat operation region between the peaks.

Computer modeling and experimental results indicated over 10 times increase in the operation frequency band of the system as compared to the conventional gyroscopes, due to the flat operating region. Thus, significantly reduced sensitivity of the gyroscope to structural and thermal parameter fluctuations and damping is achieved by eliminating mode-matching requirements. Moreover, the drawbacks of the resonance dependent approach are eliminated by utilizing dynamical amplification instead of resonance to provide large oscillation amplitudes. The prototype gyroscopes successfully demonstrated over 15 times amplification of oscillation under atmospheric pressure.

By utilizing the disturbance-rejection capability of the inertial system, improved robustness is achieved without further sophistication in control electronics. Even though the approach results in over 50% sacrifice in the gain for robustness, the observed gain is in measurable limits. Achieving improved robustness passively by the proposed design is expected to relax strict fabrication tolerances and packaging requirements, reducing production cost of micromachined gyroscopes without compromise in performance.

REFERENCES

[1] N. Yazdi, F. Ayazi, and K. Najafi. Micromachined Inertial Sensors. Proc. of IEEE, Vol. 86, No. 8, August 1998.

[2] W.A. Clark, R.T. Howe, and R. Horowitz. Surface Micromachined Z-Axis Vibratory Rate Gyroscope. Proceedings of Solid-State Sensor and Actuator Workshop, June 1994.

[3] A. Shkel, R. Horowitz, A. Seshia, S. Park and R.T. Howe. Dynamics and Control of Micromachined Gyroscopes. American Control Conference, CA, 1999.

[4] C.W. Dyck, J. Allen, and R. Hueber. Parallel Plate Electrostatic Dual Mass Oscillator. Proceedings of SPIE SOE, CA, 1999.

[5] X. Li, R. Lin, and K.W. Leow. Performance-Enhenced Micro-Machined Resonant Systems with Two-Degrees-of-Freedom Resonators. Journal of Micromech, Microeng., Vol. 10, 2000, pp. 534-539.

[6] T. Usada. Operational Characteristics of Electrostatically Driven Torsional Resonator with Two-Degrees-of-Freedom. Sensors and Actuators A, Vol. 64, 1998, pp. 255-257.

[7] E. Netzer, and I. Porat. A Novel Vibratory Device for Angular Rate Measurement. Journal of Dynamic Systems, Meas. and Control, 1995.

[8] C. Acar, A. Shkel. A Design Approach for Robustness Improvement of Rate Gyroscopes. Modeling and Simulation of Microsystems Conference, March 2001.

[9] C. Acar, A. Shkel. Microgyroscopes with Dynamic Disturbance Rejection. SPIE Conference on Smart Electronics and MEMS, March 2001.

[10] C. Acar, S. Eler, and A. Shkel. Concept, Implementation, and Control of Wide Bandwidth MEMS Gyroscopes. American Control Conference, June 2001.

[11] C. Acar, A. Shkel. Design Concept and Preliminary Experimental Demonstration of MEMS Gyroscopes with 4-DOF "Master-Slave" Architecture. SPIE Conference on Smart Electronics and MEMS, March 2002.

[12] C. Acar and A. Shkel. Wide Bandwidth Micromachined Gyroscope to Measure Rotation. Patent pending, UCI Office of Technology Alliances, Case No:2001-140-1.

[13] D.A. Koester, R. Mahadevan, B. Hardy, and K.W. Markus. MUMPs Design Handbook, Revision 5.0. Cronos Integrated Microsystems, 2000.

[14] A. Shkel, R.T. Howe, and R. Horowitz. Modeling and Simulation of Micromachined Gyroscopes in the Presence of Imperfections. International Conference on Modeling and Simulation of Microsystems, Puerto Rico, 1999, pp. 605-608.